

Atomic and electronic structure of carbon strings

S Tongay, S Dag, E Durgun, R T Senger and S Ciraci

Department of Physics, Bilkent University, 06800 Ankara, Turkey

E-mail: ciraci@fen.bilkent.edu.tr

Received 1 February 2005

Published 10 June 2005

Online at stacks.iop.org/JPhysCM/17/3823

Abstract

This paper presents an extensive study of various string and tubular structures formed by carbon atomic chains. Our study is based on first-principles pseudopotential plane wave and finite-temperature *ab initio* molecular dynamics calculations. Infinite- and finite-length carbon chains exhibit unusual mechanical and electronic properties such as large cohesive energy, axial strength, high conductance, and overall structural stability even at high temperatures. They are suitable for structural and chemical functionalizations. Owing to their flexibility and reactivity they can form linear chain, ring, helix, two-dimensional rectangular and honeycomb grids, three-dimensional cubic networks, and tubular structures. Metal–semiconductor heterostructures and various quantum structures, such as multiple quantum wells and double-barrier resonant tunnelling structures, can be formed from the junctions of metallic carbon and semiconducting BN linear chains. Analysis of atomic and electronic structures of these periodic, finite, and doped structures reveals fundamentally and technologically interesting features, such as structural instabilities and chiral currents. The double covalent bonding of carbon atoms depicted through self-consistent charge density analysis underlies the chemical, mechanical, and electronic properties.

(Some figures in this article are in colour only in the electronic version)

1. Introduction

Advances in nanoscience have opened the field of nanoelectronics, aiming at the ultimate miniaturization of electronic circuits with high speed, ultra-high component density, and novel functionalities. The main challenge of the research on molecular electronics (or moletronics) [1, 2] has been in connecting those nanodevices. To develop highly conducting interconnects, intense research has focused on nanowires [3]. Unusual mechanical and transport properties of metallic wires [4–7], in particular a close correlation between their atomic structure and stepwise variation of conductance, have been revealed [8–10]. Following predictions of several theoretical studies [11–13], the production of monatomic linear gold

chains, and chiral gold nanowires and nanotubes suspended between two gold electrodes, have been a breakthrough [14–18]. Unfortunately, thin metal wires drawn between two electrodes were not reproducible, and hence were unsuitable for device applications. Carbon nanotubes [19, 20] with their unusual mechanical and electronic properties have been considered as a promising class of nanostructures meeting several requirements and offering new paradigms in nanoelectronics. In addition to several prospective device applications [21], single-wall carbon nanotubes (SWNT) are also considered as interconnects. Experimentally and theoretically it has been shown that SWNTs can be uniformly coated with Ti atoms [22, 23].

Another ultimate one-dimensional (1D) nanowire, namely a monatomic linear chain of carbon atoms (C-LC), attracted the interest of several researchers much earlier [24–30], but has been overshadowed lately due to intense research on carbon nanotubes. Using chemical methods, production of carbon monatomic chains up to 20 atoms in length has been achieved [31]. Recently, C-LC has been observed at the centre of multi-wall carbon nanotubes [32]. Apart from being a prospective nanoscale interconnect, quasi-1D ordering of carbon atoms in the form of atomic strings provides the basis for various nanostructures [33]. Depending on their geometrical shape and dimensionality, these structures are expected to exhibit novel physical properties of technological interest.

In this study we carried out an extensive analysis of C-LC and various nanostructures based on carbon strings using first-principles calculations. Here we placed an emphasis on the electronic structure of the ring, various 2D grids and the 3D cubic network. In addition to string structures, we also considered tubular forms made by stacking of polygons (such as triangles, pentagons and hexagons) of carbon atoms on top of each other. We also examined the confined states of a superlattice heterostructure made by the periodic repetition of a $C_N(BN)_M$ linear chain. The doping of C-LC with transition metal atoms has been studied by spin-relaxed calculations, indicating the possibility of a magnetic ground state and high spin polarization at the Fermi level.

We show that carbon string structures display properties which not only make them a potential alternative to gold nanowires [16, 17] and SWNTs [21] but also point to some other applications. C-LC is a special structure of carbon with very stable and impressive mechanical properties, and is suited to structural and chemical functionalizations. We predict that it will be relatively easy to realize T and crossbar junctions, which may lead to other 2D and 3D grid and network structures. Carbon strings are flexible, but very stiff axially. Their transport properties are interesting; in spite of the fact that the parent 3D carbon crystal (namely diamond) is an insulator, an ideal C-LC is a better conductor than a linear gold chain [15]. Even though some of the structures treated in this paper are not synthesized yet, it is hoped that present findings will initiate further theoretical and experimental studies.

The paper is organized in the following manner: in the next section we describe the methods of our total energy calculations, and give the parameters used in these calculations. In section 3, we present our results concerning optimized atomic structure, self-consistent electronic structure, energetics and stability analysis for various carbon based string and tubular structures. In particular, we discuss Peierls dimerization in C-LC and second-order Jahn–Teller distortions in the ring structures together with their effects on the physical properties. Section 4 includes our concluding remarks and a brief summary.

2. Method

We have performed self-consistent field (SCF) total energy and electronic structure calculations using the first-principles pseudopotential plane wave method [34, 35] within density functional theory (DFT) [36]. All infinite- and finite-size nanostructures in our study have been treated

within supercell geometries. The generalized gradient approximation (GGA) [37] has been used to carry out spin-paired as well as spin-relaxed calculations. All the atomic positions and lattice parameters of periodic structures have been optimized by minimizing the total energy, forces on atoms, and stress on the structure. For the ultrasoft pseudopotentials [35, 38] used in our calculations the wavefunctions are represented by plane waves up to kinetic energy cut-off 400 eV. The Brillouin zones of various structures have been sampled by the Monkhorst–Pack \mathbf{k} -point special sampling scheme [39]. The number of \mathbf{k} -points is determined by performing convergence tests, which yield a $1 \times 1 \times 51$ mesh appropriate for the case of C-LC with a single atom per supercell. For larger supercells, the appropriate numbers of \mathbf{k} -points have been set by scaling them according to the size of the unit cell.

Since the stability of the structures we are predicting is relevant for applied research and future technological applications, we performed a detailed analysis of stability by re-optimizing the structures after displacing individual atoms from their original optimized configuration. Furthermore, *ab initio* molecular dynamics (MD) calculations have been carried out for all structures at high temperatures ($800 \text{ K} \leq T \leq 1200 \text{ K}$), for a large number of time steps.

3. Atomic and electronic structure, energetics, and stability

We considered a large number of carbon-based nanostructures, which are categorized into string and tubular forms. The string structures are formed based on the monatomic chain of carbon atoms. The tubular structures we consider in this work are different from single- or multi-wall carbon nanotubes. The latter are visualized by rolling of a graphene sheet on a cylinder of radius R with different chiralities and are left beyond the scope of the present study [21]. The present tubular structures are formed by stacking triangular, pentagonal, and hexagonal layers of carbon atoms in the axial direction. In figure 1 we schematically describe these structures.

3.1. Linear chain

The carbon linear chain is the precursor to all string structures. In this section we discuss its atomic structure, stability, and energy-band structure in detail. Several 1D chain structures of carbon including narrow- and wide-angle zigzags (where atoms are displaced in the direction perpendicular to the axis of the chain to form zigzags in the same plane) and dumbbell geometries have been considered. Among all these 1D chain structures C-LC, known as cumulene, is found to be the only stable structure. Upon relaxation, all other carbon chains are transformed into C-LC with a bond length of $c = 1.27 \text{ \AA}$. This finding is in contrast with the chain structures of metals [40, 41] and other group IV elements (Si, Ge, Sn) [42], where the narrow-angle zigzag structure (with an apex angle of $\sim 60^\circ$) is energetically more favourable than the linear chain structure. That the planar zigzag structure is unstable and transforms to a linear chain is indigenous to C and BN chains. Comparison of the cohesive energies of C-LC having twofold coordination and bulk diamond having fourfold coordination indicates the dramatic differences in bonding. The cohesive energy of C-LC calculated by using GGA is 8.6 eV/atom and is close to 92% of the calculated cohesive energy of bulk diamond (9.4 eV/atom). The lower coordination in C-LC is compensated by stronger bonds.

The electronic band structure and total density of states of C-LC with optimized uniform bond distances are presented in figure 2. The σ band below the Fermi energy, E_F , is composed from $2s$ and $2p_z$ atomic orbitals. The doubly degenerate π band is formed from the bonding combinations of $2p_x$ and $2p_y$ atomic orbitals. This band crosses E_F at $k = \pi/2c$ and hence accommodates two electrons per unit cell. In addition to the σ band derived from the states of the σ band, doubly degenerate half-filled [$\pi(2p_x)$ and $\pi(2p_y)$] band states are combined

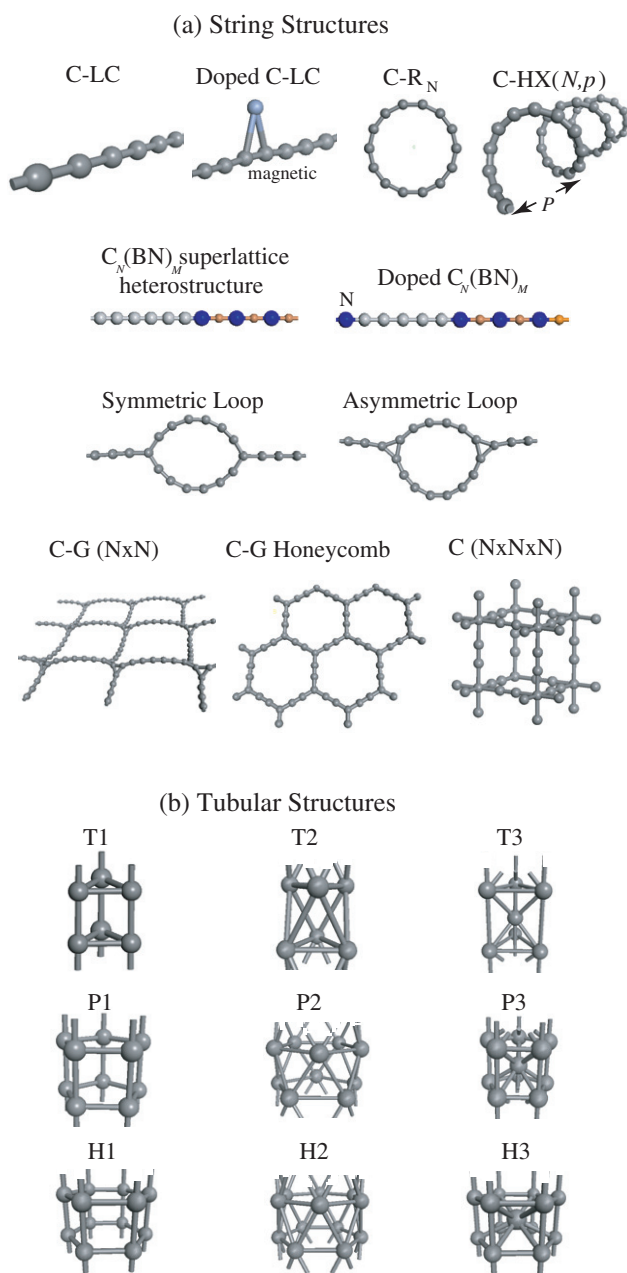


Figure 1. (a) Nanostructures based on carbon strings: carbon linear chain (C-LC); doped C-LC; ring structure of N carbon atoms (C-R $_N$); helix structure having N atoms per pitch length p (C-HX(N,p)); C $_N$ (BN) $_M$ superlattice; N- or B-doped C $_N$ (BN) $_M$ superlattice; symmetric and asymmetric loop devices; 2D rectangular and honeycomb grids; 3D cubic network. (b) Tubular structures: T1, P1, and H1 tubes are made of respectively, triangular, pentagonal, and hexagonal layers of carbon stacked in top-to-top configuration. In T2, P2, and H2 the layers are staggered. T3, P3, and H3 structures have extra carbon atoms in between the layers.

to form another π bond. The double-bond structure is visualized by the plots of band charge densities presented in figure 2(c).

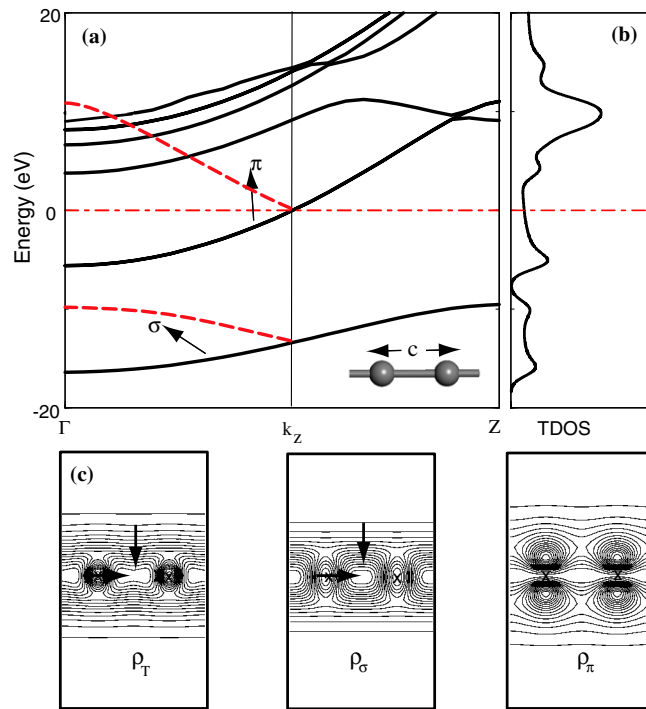


Figure 2. Energy band structure of C-LC with uniform bond distance $c = 1.27 \text{ \AA}$ (a), and corresponding total density of states (TDOS) (b). The dashed lines denote zone folded bands. The zero of energy is set at the Fermi level. (c) Charge contour plots of C-LC. Total charge density, ρ_T , and charge density corresponding to σ and π bonds are shown on a plane containing the axis of the chain. The arrows indicate the direction of increasing charge density.

This double-bond structure contributes a highly metallic character to C-LC, and the elastic stiffness defined as the second derivative of the strain energy per atom with respect to the axial strain, $d^2E/d\epsilon^2$, is calculated to be as high as 119 eV in C-LC. On the other hand, the dimensionality as well as the type of the π band make C-LC vulnerable to Peierls distortion. According to the well known Peierls theorem [43] the metallic chain of equidistant atoms can be expected to undergo a distortion by doubling the size of the unit cell of the periodic structure. The instability occurs through folding of the bands at the $k = \pi/2c$ point and opening of a gap at the Fermi level, as shown in figure 3(c). Once alternating carbon atoms in the C-LC are displaced by δ in the same direction (by forming an alternating sequence of long and short bonds resulting in a dimerization), the unit cell size is doubled, and folded π bands are split at E_F . The gain of energy through the lowering of the occupied π band around the $k = \pi/2c$ -point is the driving force for the Peierls distortion, which may induce a metal–insulator transition.

Whether LDA calculations can lead to the Peierls distortion in C-LC has been a subject of several studies [30]. The predictions of the theory regarding the strength of this many-body effect strongly depends on the methodology used. Here, using LDA and GGA we calculate the change of energy per unit cell with the displacement of every other carbon atom in the chain as a result of dimerization. The energy-change profiles obtained by using GGA and LDA both display a minimum at $\delta \approx 0.017 \text{ \AA}$ (see figure 3(a)). The energy gain per atom through distortion is calculated to be just 2.7 and 3.2 meV with LDA and GGA, respectively.

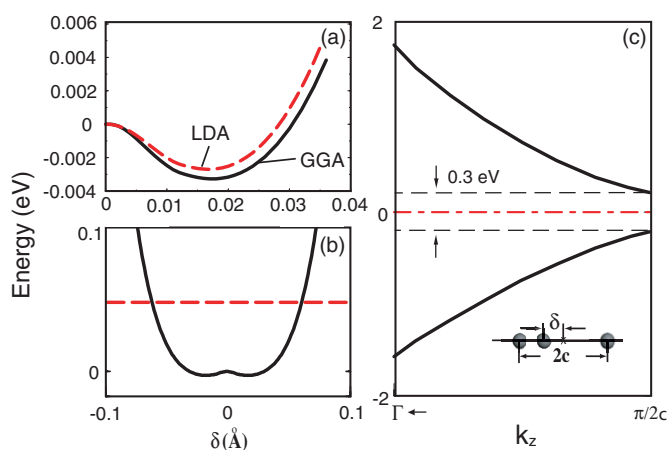


Figure 3. Peierls distortion in C-LC: (a) GGA- and LDA-calculated effective double-well potential with minima at $\delta \approx \pm 0.017$ Å. (b) The zero-point oscillation energy of a C atom (denoted by the dashed line) in the GGA-calculated effective potential. (c) Gap opening of the zone-folded π band at $k = \pi/2c$ upon doubling of the chain periodicity by the dimerization of the chain.

These results imply that in fact LDA and GGA give rise to an insignificant Peierls distortion in C-LC. Treating the GGA-calculated energy-change profile as an effective potential for the dynamics of a C atom in the chain, the ground state energy of the atom in the double-well potential turns out to be 51 meV. Clearly the zero-point energy is much higher than both the Peierls distorted ground state energy and the energy of the metallic state. As a result, Peierls distortion cannot be observed even at $T = 0$ K with the GGA and LDA energies. On the other hand, we note that the *ab initio* Hartree–Fock (HF) calculations predict the displacement of the alternating C atoms to be almost ten times as large, and the effective potential to be 60 times as deep as LDA results. However, from studies on the bond alternation effect (i.e. second-order Jahn–Teller effect) in carbon ring structures, it is known that while LDA and GGA somewhat underestimate the effect, the HF method tends to overestimate it [28, 29]. Another interesting point to note is that although Si and C are isovalent elements the σ band dipping below the Fermi level delocalizes the double-bond structure, and prevents the Si linear chain from undergoing Peierls distortion [42].

3.2. Rings and helices

The axial strength and radial flexibility of the monatomic carbon chain led us to consider some other related carbon structures having curved forms such as rings and helices as schematically depicted in figure 1. Closed circular forms of carbon atomic chains (or planar monocyclic rings), C- R_N as we label them, are synthesized experimentally up to relatively large sizes with $N \sim 30$, and studied both experimentally and theoretically [25–29]. The properties of C- R_N planar ring structure depend strongly on the value of N , whether N is odd, $N = 4n$, or $N = 4n + 2$ (n being a natural number). For $N = 4n + 2$, the electron correlation appears to be decisive in the stability of the structure. According to the Hückel rule the double π -electron conjugation is responsible for the strong aromatic stabilization. C- R_N tends to favour one of the three structural forms: in the A-structure, (i.e. monocyclic cumulenic) having D_{Nh} symmetry, all bond lengths and bond angles are equal. Within the $D_{(N/2)h}$ symmetry either the B-structure with bond-angle alternation or the (polyacetylenic) C-structure with bond-

Table 1. Structural type (A, equal bond lengths and angles; B, bond angle alternation; C, bond-length alternation), binding energy (E_b), and energy gap between LUMO and HOMO (E_g) of carbon rings, C-R $_N$, for $N = 8, 10, \dots, 30$.

N	8	10	12	14	16	18	20	22	24	26	28	30
Type	B, C	B	B, C	A	C	A	C	A	C	A	C	A
E_b (eV)	7.45	7.93	7.89	8.12	8.07	8.20	8.16	8.24	8.21	8.26	8.24	8.27
E_g (eV)	1.1	3.6	0.9	2.7	0.9	2.2	0.8	1.9	0.7	1.6	0.6	1.4

length alternation is favoured [29]. It appears that the competition between this conjugated aromaticity, second-order Jahn–Teller and Peierls instabilities (for very large N) determines the type of structure. Small carbon rings with $3 \leq N \leq 7$ have been treated by Saito and Okamoto [28] using the hybrid DFT method. Jones and Seifert [25] carried out calculations for $14 \leq N \leq 24$ using HF and second-order Moller–Plesset calculations. They found that C-R $_N$ rings with $N = 14, 18, 22$ are in the A-structure, and those with $N = 16, 20, 24$ are in the C-structure. Calculations by Torelli and Mitas [29] have revealed that while HF calculations predict rings with $N = 10, 14, 18$ to be in the C-structure, multi-configuration self-consistent field calculations refute the bond alternation in C-R $_{10}$.

In this study, we examined C-R $_N$ planar ring structures having even numbers of atoms in the range $8 \leq N \leq 30$ within DFT and GGA. Although fine details of C-R $_N$ depend on proper treatment of many-body effects, our objective is to reveal broad features such as energetics and electronic energy structure within DFT. For odd N , the ring is distorted so that all bond lengths become non-uniform. The details of atomic and electronic structures of carbon rings and their energetics are summarized in table 1. Remarkably, we found that the C-R $_{10}$ ring is in the B-structure. Bond lengths remain uniform, but bond angles alternate with $\alpha = 131^\circ$ and 157° . On the other hand, we found that C-R $_{12}$ exhibits alternations in bond length as well as in bond angle. As compared to the state of the A-structure this corresponds to an energy gain of 87 meV/atom, which is 54 times larger than the energy gain due to the Peierls distortion of C-LC. The inset in figure 4 illustrates the effective potential obtained by the circumferential displacement δ of every other atom in C-R $_{12}$. As shown, the ground state energy associated with the longitudinal vibration of carbon atoms is located close to the bottom of this effective potential, which has a double-well form. Therefore, the bond alternations of C-R $_{12}$ should be observable even at room temperature. As seen in table 1 all C-R $_N$ ring structures with $N = 4n$ are found in the C-structure, if $N > 12$, whereas those with $N = 4n + 2$ are in the A-structure. The variation of the binding energy, E_b , and the gap between the energies of the LUMO and HOMO, E_g , with N are illustrated in figure 4. The binding energy E_b of C-R $_N$ should increase with increasing N due to decreasing strain, but it displays an oscillatory variation. We observe the interesting trend $E_b[N = 4n + 2] > E_b[N = 4(n + 1)]$. As $N \rightarrow \infty$, E_b approaches the asymptotic value of 8.6 eV, namely the binding energy of C-LC. The LUMO–HOMO gap exhibits a similar relation, $E_g[N = 4n + 2] > E_g[N = 4(n + 1)]$, but the overall trend is opposite: E_g decreases with increasing N . The calculated energy level diagram of C-R $_{12}$ is illustrated in figure 5.

Similar to the ring structure, single helical strands of carbon are also found to be stable. The helix structure generated from carbon strings can occur in different radii and pitch lengths. We denote the helix structure by C-HX $_{(N,p)}$ where N is the number of C atoms in one pitch (p , in Å) of the helix. In the configurational space of (N, p) , periodic (infinite length) helix structure stays in a very flat potential, and hence does not show a strong tendency to transform into a linear chain. On the other hand, a finite helix structure is stabilized by fixing from both ends. The binding energy of C-HX $_{(N,p)}$ depends on N and p . For example, for a fixed pitch length $p = 10$ Å, E_b is 8.3 and 8.5 eV for $N = 10$ and 16, respectively. The binding energies

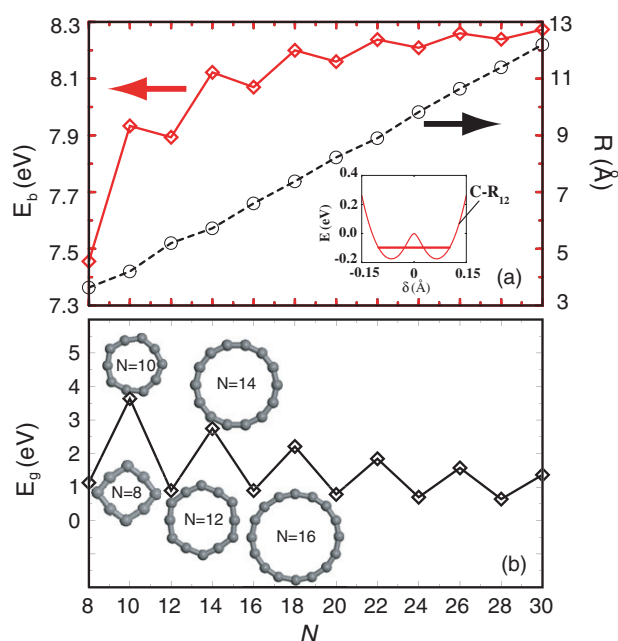


Figure 4. (a) Variation of binding energy, E_b (eV/atom), and radius R (Å) of $C-R_N$ with number of carbon atoms N . (b) LUMO–HOMO energy gap, E_g , of $C-R_N$ as a function of N . The inset shows the zero-point energy of longitudinal vibrations of a carbon atom in the effective potential associated with the bond alternation in $C-R_{12}$.

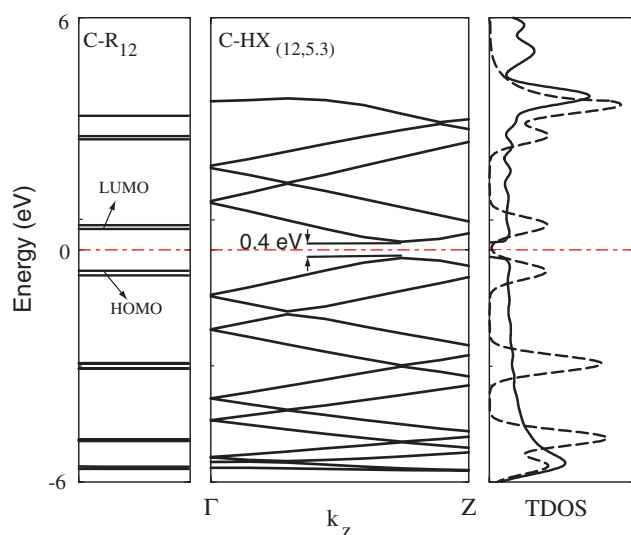


Figure 5. Calculated energy level diagram of $C-R_{12}$, and energy band structure of $C-HX_{(12,5,3)}$. The corresponding TDOS of the ring and the helix are shown by dashed and solid curves, respectively.

are slightly smaller than that of the C-LC due to strain energy implemented by the curvature, but they approach it with increasing radius and/or p . All C-HX structures we studied here have the bond alternation no matter what the value of N is, and are stable even at $T = 1200$ K. In figure 5 the electronic band structure and TDOS of $C-HX_{(12,5,3)}$ are shown. The electronic structure is a kind of combination of the electronic structures of C-LC and $C-R_N$. The bands are formed due to the periodic structure with lattice parameter $c = p$. Owing to the band formation, the LUMO–HOMO energy gap of $C-R_{12}$ has reduced to 0.4 eV in the $C-HX_{(12,5,3)}$ structure. We believe that the helix structure may be interesting to study chiral currents and to fabricate nanosolenoids. Transport properties of helix structure are discussed in [33].

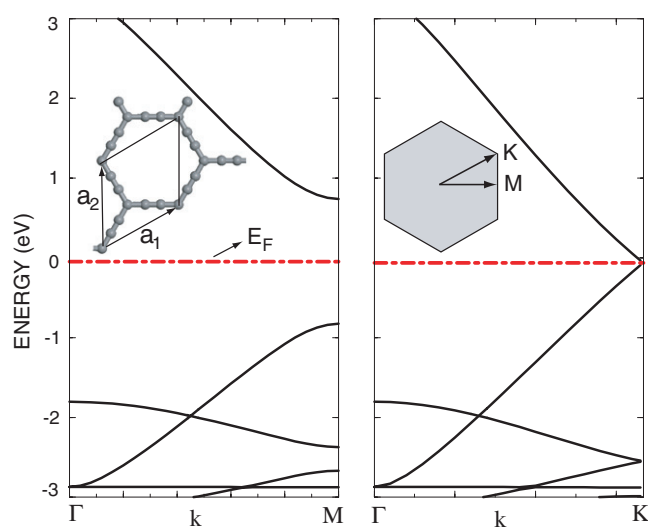


Figure 6. Calculated energy band structure of the carbon honeycomb structure having four atoms per edge. The primitive unit cell and the corresponding Brillouin zone are shown as insets.

A special case for the ring structure is the symmetric or asymmetric loop described in figure 1(a). For the symmetric loop, the junction to C-LC is achieved by the sp^2 -bands and the circular cross section becomes oblique. The asymmetry of the junction with C-LC is expected to lead to interesting consequences in quantum conduction.

3.3. 2D honeycomb grid and 3D cubic network

Earlier we have shown that C-LC can branch off to form T junctions (C-T) and crossbar junctions (C-CB) [33]. These junctions can form because an additional carbon atom can easily be attached to any carbon atom of C-LC with a significant binding energy (see section 3.4). For example, a T junction is produced if a perpendicular chain develops from that adatom. At the junction the double-bond structure changes into planar sp^2 -like bonding with equal 120° angles between the bonds. In the case of the crossbar junction, one carbon atom in the linear chain is connected to two adjacent atoms in the same chain and also to two carbon atoms of the crossing chain. This way, a tetrahedral coordination and hence 3D sp^3 -like bonding are achieved at the junction. The stable T and crossbar junctions have been exploited to form 2D grid and 3D network structures. First, we examine the 2D C-G($N \times N$) square grids having $N = 6$ and 9. Owing to the 3D sp^3 -like bonding at the corners, the C-G($N \times N$) square grids are neither perfectly planar, nor made of perfect squares. For example, the C-G(6×6) grid, which initially incorporates six carbon atoms along each edge of the square and has nine atoms in the 2D cell, deviates from planar square geometry upon relaxation. *Ab initio* molecular dynamics calculations performed at $T = 800$ K have confirmed the stability of the grid structures. The grid structures with larger N , for example C-G(9×9), shared similar overall atomic configurations and stabilities. The electronic structure calculated self-consistently along the edges of squares indicates that $N = 6$ and 9 square grids are semiconductors. However, the bandgap decreases as N increases. We found also that N being even or odd affects the overall shape of the bandgap. For example, while C-G(9×9) is an indirect bandgap semiconductor, C-G(6×6) has a direct bandgap. The semiconducting behaviour is associated with the sp^3 -like bonding at the corners of the grid. The situation is, however, different for the 2D honeycomb grid. The 2D hexagonal primitive unit cell is illustrated in figure 6 as an inset. Since the carbon atoms at the corners of the hexagons form sp^2 -bonding, the structure is planar and is

graphene-like. The electronic structure of the honeycomb structure having four carbon atoms along each edge of the hexagon is reminiscent of that of the graphene. It is metallic since π and π^* bands cross the Fermi level at the corner of the first Brillouin zone. The calculated electronic band structure of the stable honeycomb grid is presented in figure 6.

A 3D ($4 \times 4 \times 4$) cubic network as described in figure 1(a) is found to be stable at $T = 0$ K, but deformed and clustered at $T = 500$ K. The structure corresponding to $T = 0$ K is found to be metallic with a single band crossing the Fermi level for \mathbf{k} which are parallel to the edges of the cube. Improving the stability of the cubic network by substituting the corner atoms with atoms having six valence electrons, such as S, Se, and Te, is crucial for further understanding. While carbon grid and network structures have not been produced yet, present calculations indicate that they can be stable at reasonable temperatures. Through different geometries and structural variations such as N and periodic doping, these structures offer several possibilities to engineer their physical properties. Since they incorporate nodes and metallic interconnects, one can contemplate that these structures may be used in the future for device integration in molecular electronics.

3.4. Functionalizations of carbon strings

Carbon chains are reactive owing to their double-bond structure. As possible mechanisms of functionalizing carbon strings we have considered chemisorption and substitution of foreign atoms, and investigated the effects on their electronic and magnetic properties. As far as the branching of C-LC is concerned, the adsorption of an individual carbon atom in the C-LC is crucial. First we consider the adsorption of a single carbon atom at a top-site of the chain. The binding energy is calculated to be 4.9 eV. The presence of the additional carbon atom modifies the bonding locally to sp^2 . An oxygen atom can also be chemisorbed to a single carbon atom of C-LC, or to two adjacent carbon atoms to form a bridge bond. The former is found to be energetically favourable by 0.2 eV and has binding energy of ~ 5 eV. Similarly, a single hydrogen atom can easily be adsorbed to a chain atom with $E_b = 3.6$ eV. Hydrogen is chemisorbed on the surfaces of SWNTs with relatively smaller binding energy [44]. Here, at the chemisorption site the bonding configuration changes from double-bond structure to planar sp^2 -like as in a C-T junction. By attaching another H atom to the same carbon from the opposite side the 2D sp^2 -like bonding changes to 3D sp^3 -like bonding. A $(CH_2)_n$ structure develops if this procedure is repeated for each carbon atom of the chain. Consequently, the double-bond structure of the carbon chain is lost, and the metallic C-LC becomes a wide bandgap semiconductor.

In addition to the external doping of C, O (bridge and top site adsorption), and H, we also examined adsorption of Al, Si, S, Mn, Fe, Co, and Cr atoms on C-LC, and N, O, P, S, Al, and Si atoms as substitutional impurities in C-LC. In these calculations, a foreign atom A is adsorbed on the top or bridge site and this configuration is repeated periodically to have the C_5A formula per cell. We treated the substitutional impurity within the supercell geometry by replacing one carbon atom with a foreign atom A in each six-carbon atom segment of C-LC. In table 2 we present our results for external doping of C-LC by foreign atoms. The electronic structure of the C-LC is affected by the external or substitutional impurity atoms. Upon adsorption of transition metal (TM) atoms on C-LC, the ground state of the system becomes a ferromagnetic metal. Spin-relaxed GGA calculation of a TM atom adsorbed on C-LC yields a net magnetic moment and a lower total energy than that obtained from spin-paired GGA. The densities of states for the majority and minority spins at the Fermi level (i.e. $D_\uparrow(E_F)$ and $D_\downarrow(E_F)$, respectively) are of particular importance. The spin polarization is defined as $P = (D_\uparrow(E_F) - D_\downarrow(E_F)) / (D_\uparrow(E_F) + D_\downarrow(E_F))$. The larger P at the Fermi level, the more important is the structure in spintronic applications. In figure 7 we show the calculated

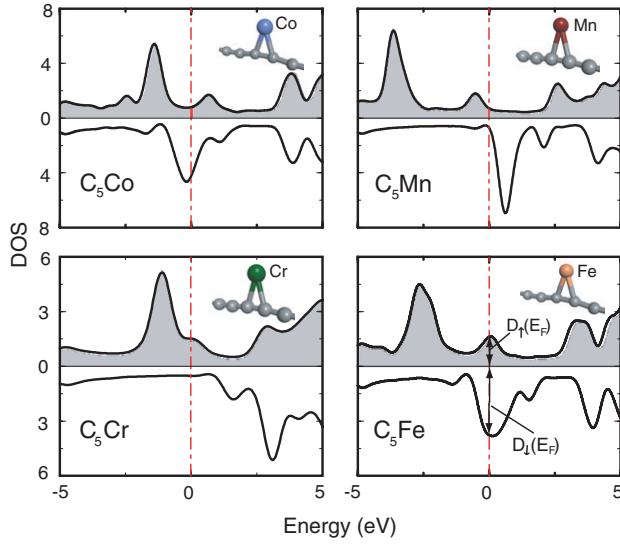


Figure 7. Calculated state densities of majority (shaded) and minority spin states of C-LC doped periodically and externally with Co, Mn, Cr and Fe atoms. Geometrical configurations of adsorption are shown as insets. Spin polarization at E_F becomes prominent only when the difference between the densities of states of majority and minority spins, $D_{\uparrow}(E_F) - D_{\downarrow}(E_F)$, becomes significant.

Table 2. Results of the adsorption or external doping of foreign atoms on the C-LC. Binding site (T = top, B = bridge site); binding energy E_b of foreign atom; magnetic moment μ per unit cell in Bohr magnetons; distance to nearest carbon atoms of the C-LC, d_1 and d_2 . Each supercell includes five carbon atoms and one foreign atom.

Compound	Site	E_b (eV)	μ (μ_B)	d_1 (Å)	d_2 (Å)
C ₅ Si	T	3.2	—	1.8	2.1
C ₅ Si	B	3.1	—	1.9	2.9
C ₅ Mn	B	0.9	5.6	2.2	2.9
C ₅ Fe	B	1.3	3.3	2.0	2.8
C ₅ Cr	B	1.0	5.1	2.2	2.9
C ₅ Co	B	1.6	1.4	1.9	2.7
C ₅ Al	B	2.2	—	2.2	2.8
C ₅ Ti	B	2.6	1.5	2.0	2.2

densities of majority and minority spin states of TM atom doped C-LC. Significant values of polarization are achieved in cases of external adsorption of Co and Fe atoms.

3.5. Superlattice of heterostructures

We next examine heterostructures formed by the junctions of C-LC and BN-LC. Boron nitride, being a III-V compound, can form stable linear string structure and display properties very similar to that of C-LC, except that it is a wide bandgap insulator. The bandgap of BN-LC has been calculated to be 5 eV. Normally, a long C-LC–BN-LC chain is a metal–semiconductor junction. A periodic arrangement of $C_N(BN)_M$ forms a superlattice. It is interesting to know how 1D superlattices can differ from those in 3D, and whether the periodic arrangement of metal–insulator heterostructure gives rise to multiple quantum-well structures. In the past, metal–semiconductor junctions (such as Al–Si) and the nature of the Schottky barrier at their interface have been subjects of intense research. Here we investigate the $C_N(BN)_M$ superlattice with fully optimized structure. Calculated energy band structures indicate that these superlattices are semiconductors. The bandgap is, however, a strong function of N and M . For example, we found the bandgap $E_g = 1.2, 1.6, 1.8$ eV for the superlattices with $N = 6$

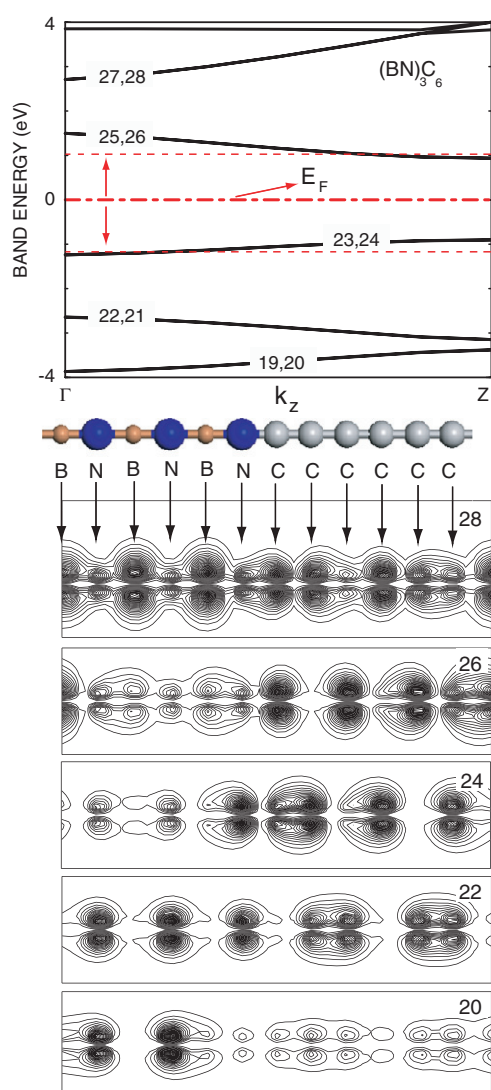


Figure 8. Calculated energy band structure of the $(\text{BN})_3\text{C}_6$ superlattice is presented in the top panel. Numerals are band indices. As shown by arrows, the substitution of a carbon atom by a single B or N shifts the Fermi level down or up to metallize the superlattice. The charge density contour plots of various bands below and above the Fermi level E_F are presented in the lower panels.

and $M = 1, 2, 3$, respectively, suggesting that E_g increases with increasing M . While $\text{C}_6(\text{BN})_3$ has a bandgap of 1.8 eV, the bandgaps of $\text{C}_{12}(\text{BN})_3$ and $\text{C}_{15}(\text{BN})_3$ are 1.1 and 0.8 eV, respectively. It appears that E_g also decreases with increasing N . In figure 8 we present the energy band structure of the $(\text{BN})_3\text{C}_6$ superlattice. While the superlattice is a semiconductor, the substitution of C atoms with single B (or N) pushes the Fermi level down (or up) as shown in figure 8 to metallize the superlattice.

The character of the bands of the $(\text{BN})_3\text{C}_6$ below and above the Fermi level is analysed by charge density contour plots on a plane passing through the axis of the superlattice. The doubly degenerate highest valence and the lowest conduction bands are derived from the doubly degenerate π^* band of C-LC. These states are confined in the C-LC region of the superlattice, since their energies fall in the bandgap of BN-LC. Second highest filled and lowest empty bands appear to have more weight on the BN-LC site. However, bands $n = 20$ and 30 are confined on the $(\text{BN})_3$ -site, since these band states cannot match states in the C-LC site. The

absence of the Bloch states having wavevector perpendicular to the chain axis is a profound difference between 1D and bulk heterostructures. In the present case, states of the superlattice tend to be confined to either the C-LC or the BN-LC site.

3.6. Carbon tubular structures

Some possible tubular structures of carbon atoms (excluding carbon nanotubes) are depicted in figure 1(b). These structures are different from the carbon-string-based structures discussed above, since their cross section perpendicular to their axis is formed of polygons (triangle, pentagon and hexagon) of carbon atoms. In figure 1(b) the three tubular structures in the first row, i.e. T_1 , T_2 , T_3 are made of triangles having carbon atoms at their corners, which are stacked along the axis of the tube. In T_1 , triangles are identical; in T_2 , they are staggered; in T_3 structure, additional carbon atoms are located in between parallel triangles. We followed the same convention for pentagonal (P_1 , P_2 , P_3) and hexagonal (H_1 , H_2 , H_3) tubular structures. We found that all T_3 , P_3 , H_3 structures are unstable and transform to diamond-like clusters. T_1 is also unstable and it transforms to three C-LCs with repulsive interactions. As for T_2 , during structural optimization it first transforms to T_1 by rotation of every other triangle by 60° , then disintegrates to three parallel C-LCs.

The P_1 is stable with a binding energy $E_b = 7.47$ eV and all C–C bond distances become $d_{C-C} \sim 1.5$ Å. This structure corresponds to a local minimum and it is a semiconductor with $E_g = 0.7$ eV. Similarly, H_1 is a stable structure with $E_b = 7.42$ eV, $d_{C-C} \sim 1.5$ Å, but it is a metal with calculated ideal conductance of $G = 6G_0$. Both P_2 and H_2 are unstable and transform to P_1 and H_1 , respectively.

4. Conclusions

In this paper, we have presented a study of various nanostructures which are derived from carbon strings. These structures show interesting mechanical and electronic properties. The monatomic linear chain of carbon atoms is the basic structure, which is precursor to other more complex structures we studied. While diamond with sp^3 covalent bonding is an insulator, the linear carbon chain having uniform bond length is a good conductor. That it is flexible, but has very high axial strength, causes the carbon chain to exhibit a string-like behaviour. The stable, planar, and monocyclic ring structures comprising different numbers of atoms, and helix structures, originate from string behaviour of the carbon linear chain. All these structures have interesting electronic structures and structural instabilities, which modify ideal geometries by inducing bond length and/or bond angle alternations, lowering the total energy of the systems. Carbon string structures also exhibit high chemical activity to various atoms. This property makes them suitable for functionalizations. We investigated external adsorption and substitution of foreign atoms in C-LC, yielding interesting electronic and magnetic properties. We also studied the C-LC and BN-LC heterostructure superlattices, yielding electronic structures suitable for bandgap engineering in 1D systems. The double-bond structure between adjacent carbon atoms is found to underlie all these unusual physical and chemical properties. Formation of T and crossbar junctions from carbon strings can be crucial for nanotechnology. In this study, we examined $(N \times N)$ rectangular and also honeycomb grids. We also considered the $(N \times N \times N)$ cubic network. As far as technological applications of interconnects or nanodevices are concerned, the transport properties of carbon string structures are of particular interest.

Acknowledgment

SC acknowledges partial support by TÜBA (The Academy of Sciences of Turkey).

References

- [1] Aviran A and Ratner M A 1974 *Chem. Phys. Lett.* **29** 277
- [2] Roth S and Joachim C 1997 *Atomic and Molecular Wires* (Dordrecht: Kluwer)
Jortner J and Ratner M A (ed) 1997 *Molecular Electronics* (Oxford: Blackwell)
- [3] Joachim C, Gimzewski J K and Aviram A 2000 *Nature* **408** 541
- [4] Agraït N, Rodrigo J G and Vieira S 1993 *Phys. Rev. B* **47** 12345
- [5] Pascual J I, Mendez J, Gomez-Herrero J, Baro A M, Garcia N and Binh V T 1993 *Phys. Rev. Lett.* **71** 1852
- [6] Krans J M, Müller C J, Yanson I K, Govaert T C M, Hesper R and Van Ruitenbeek J M 1993 *Phys. Rev. B* **48** 14721
- [7] For a recent review of the subject see, Ciraci S, Buldum A and Batra I P 2001 *J. Phys.: Condens. Matter* **13** R537
- [8] Ciraci S and Tekman E 1989 *Phys. Rev. B* **40** 11969
- [9] Agraït N, Rubio G and Vieira S 1995 *Phys. Rev. Lett.* **74** 3995
- [10] Stalder A and Dürig U 1996 *Appl. Phys. Lett.* **68** 637
- [11] Mehrez H and Ciraci S 1997 *Phys. Rev. B* **56** 12632
- [12] Gulseren O, Ercolessi F and Tosatti E 1998 *Phys. Rev. Lett.* **80** 3775
- [13] Sorensen M R, Brandbyge M and Jacobsen K W 1998 *Phys. Rev. B* **57** 3283
- [14] Ohnishi H, Kondo Y and Takayanagi K 1998 *Nature* **395** 780
- [15] Yanson A I, Bolliger G R, van der Brom H E, Agraït N and van Ruitenbeek J M 1998 *Nature* **395** 783
- [16] Kondo Y and Takayanagi K 2000 *Science* **289** 606
- [17] Oshima Y, Onga A and Takayanagi K 2003 *Phys. Rev. Lett.* **91** 205503
- [18] Senger R T, Dag S and Ciraci S 2004 *Phys. Rev. Lett.* **93** 196807
- [19] Iijima S 1991 *Nature* **354** 56
Iijima S, Ichihashi T and Ando Y 1992 *Nature* **356** 776
- [20] Dresselhaus M S, Dresselhaus G and Eklund P C 1996 *Science of Fullerenes and Carbon Nanotubes* (San Diego, CA: Academic)
- [21] For a recent review on the electronic properties see Ciraci S, Dag S, Yildirim T, Gulseren O and Senger R T 2004 *J. Phys.: Condens. Matter* **16** R901
- [22] Dai H, Wong E W, Lu Y Z, Fan S and Lieber C M 1995 *Nature* **375** 769
Zhang Y and Dai H 2000 *Appl. Phys. Lett.* **77** 3015
Zhang Y, Franklin N W, Chen R J and Dai H 2000 *Chem. Phys. Lett.* **331** 35
- [23] Dag S, Durgun E and Ciraci S 2004 *Phys. Rev. B* **69** 121407(R)
- [24] Karpfen A 1979 *J. Phys. C: Solid State Phys.* **12** 3227
- [25] Jones R O and Seifert G 1997 *Phys. Rev. Lett.* **79** 443
- [26] Wakabayashi T, Kohno M, Achiba Y, Shiromaru H, Momose T, Shida T, Naemura K and Tobe Y 1997 *J. Chem. Phys.* **107** 4783
- [27] Bylaska E J, Weare J H and Kawai R 1998 *Phys. Rev. B* **58** R7488
- [28] Saito M and Okamoto Y 1999 *Phys. Rev. B* **60** 8939
- [29] Torelli T and Mitas L 2000 *Phys. Rev. Lett.* **85** 1702
- [30] Abdurahman A, Shukla A and Dolg M 2002 *Phys. Rev. B* **65** 115106
- [31] Roth G and Fischer H 1996 *Organometallics* **15** 5766
- [32] Zhao X, Ando Y, Liu Y, Jinno M and Suzuki T 2003 *Phys. Rev. Lett.* **90** 187401
- [33] Tongay S, Senger R T, Dag S and Ciraci S 2004 *Phys. Rev. Lett.* **93** 136404
- [34] Payne M C, Teter M P, Allen D C, Arias T A and Joannopoulos J D 1992 *Rev. Mod. Phys.* **64** 1045
- [35] Numerical calculations have been carried out by using vasp software package: Kresse G and Hafner J 1993 *Phys. Rev. B* **47** 558
Kresse G and Furthmüller J 1996 *Phys. Rev. B* **54** 11169
- [36] Hohenberg P and Kohn W 1964 *Phys. Rev. B* **136** B864
Kohn W and Sham L J 1965 *Phys. Rev.* **140** A1133
- [37] Perdew J P, Burke K and Ernzerhof M 1996 *Phys. Rev. Lett.* **77** 3865
- [38] Vanderbilt D 1990 *Phys. Rev. B* **41** 7892
- [39] Monkhorst H J and Pack J D 1976 *Phys. Rev. B* **13** 5188
- [40] Sanchez-Portal D, Artacho E, Junquera J, Ordejon P, Garcia A and Soler J M 1999 *Phys. Rev. B* **83** 3884
- [41] Sen P, Ciraci S, Buldum A and Batra I P 2001 *Phys. Rev. B* **64** 195420
- [42] Tongay S, Durgun E and Ciraci S 2004 *Appl. Phys. Lett.* **85** 6179
- [43] Peierls R E 1955 *Quantum Theory of Solids* (Oxford: Clarendon) p 155
- [44] Gülseren O, Yildirim T and Ciraci S 2001 *Phys. Rev. Lett.* **87** 116802